

Manuscript Number:

Title: Numerical investigation of vortex-induced motions of a paired-column semi-submersible in currents

Article Type: VSI: Marine CFD

Keywords: Vortex-induced motions; paired-column semi-submersible; detached-eddy simulation; overset grid; naoe-FOAM-SJTU solver

Corresponding Author: Professor Decheng Wan, Ph.D.

Corresponding Author's Institution: Shanghai Jiao Tong University

First Author: Weiwen Zhao, PhD

Order of Authors: Weiwen Zhao, PhD; Lu Zou, PhD; Decheng Wan, Ph.D.; Zhiqiang Hu, Dr

Abstract: Vortex-induced motions (VIM) is becoming a noteworthy issue for column-stabilized floating platforms, mainly due to its substantial fatigue damage to risers and mooring system. The VIM of deep-draft semi-submersible is more complex than single column floaters because of the wake interference between columns, as well as the considerable yaw motions. In the present work, a numerical approach for simulating VIM of deep-draft semi-submersible is proposed. Specifically, detached-eddy simulation is used for turbulence modeling and dynamic overset grid technique is used for moving objects. Simulations for stationary drag and VIM of a model-scale paired-column semi-submersible are conducted with the proposed approach. The numerical results are compared with experimental data. Transverse, in-line and yaw motions are allowed during VIM simulations and are further analyzed in frequency domain by Fast Fourier Transform (FFT). Different VIM characteristics are observed at different current velocities. The work done by each component of the structure is also discussed. Flow visualizations are presented for better understanding of the wake interferences during VIM. The accuracy and reliability of the current numerical approach is assessed.

Suggested Reviewers: Shixiao Fu PhD
Professor, Shanghai Jiao Tong University
shixiao.fu@sjtu.edu.cn
Prof. Shixiao Fu is expert of VIM analysis.

Changhong Hu PhD
Professor, Kyushu University, Japan
hu@riam.kyushu-u.ac.jp
Prof. Changhong Hu is famous expert of CFD on marine hydrodynamics.

Qing Xiao PhD
Reader, Strathclyde University, UK
qing.xiao@strath.ac.uk
Dr. Qing Xiao is expert of CFD on and FSI and marine hydrodynamics.

Dear Atilla and Editor,

It is our pleasure to submit our recent finished paper with title "Numerical investigation of vortex-induced motions of a paired-column semi-submersible in currents" to Ocean Engineering. Thanks for your kind review and consideration of publication in Ocean Engineering.

Best regards,

Decheng

--

Prof. Dr. Decheng Wan
Chair Professor of Chang Jiang Scholars
Head of Computational Marine Hydrodynamics Lab
School of Naval Architecture, Ocean and Civil Engineering
Shanghai Jiao Tong University (SJTU)
Dongchuan Road 800
Shanghai 200240
China

Highlights:

1. Perform numerical investigations of VIM of deep-draft paired-column semi-submersible.
2. Present spectral analysis of motion responses by Fast Fourier Transform (FFT).
3. Pontoon is responsible for mitigating VIM.
4. Reveal the synchronized vortex shedding around upstream columns in lock-in range.
5. Flow reattachments are responsible for amplifying VIM.

1 1 **Numerical investigation of vortex-induced motions of a**
2
3
4 2 **paired-column semi-submersible in currents**
5
6 3 Weiwen Zhao¹, Lu Zou¹, Decheng Wan^{1*}, Zhiqiang Hu²
7
8 4 ¹*State Key Laboratory of Ocean Engineering, School of Naval Architecture, Ocean and Civil*
9 5 *Engineering, Shanghai Jiao Tong University, Collaborative Innovation Centre for Advanced Ship*
10 6 *and Deep-Sea Exploration, Shanghai, China*
11 7 ²*School of Marine Science & Technology, Newcastle University, Newcastle upon Tyne, UK*
12 8 *Corresponding author: dcwan@sjtu.edu.cn
13
14
15
16
17 10 Abstract
18
19 11 Vortex-induced motions (VIM) is becoming a noteworthy issue for column-stabilized floating
20
21 12 platforms, mainly due to its substantial fatigue damage to risers and mooring system. The VIM of
22
23 13 deep-draft semi-submersible is more complex than single column floaters because of the wake
24
25 14 interference between columns, as well as the considerable yaw motions. In the present work, a
26
27 15 numerical approach for simulating VIM of deep-draft semi-submersible is proposed. Specifically,
28
29 16 detached-eddy simulation is used for turbulence modeling and dynamic overset grid technique is
30
31 17 used for moving objects. Simulations for stationary drag and VIM of a model-scale paired-column
32
33 18 semi-submersible are conducted with the proposed approach. The numerical results are compared
34
35 19 with experimental data. Transverse, in-line and yaw motions are allowed during VIM simulations
36
37 20 and are further analyzed in frequency domain by Fast Fourier Transform (FFT). Different VIM
38
39 21 characteristics are observed at different current velocities. The work done by each component of
40
41 22 the structure is also discussed. Flow visualizations are presented for better understanding of the
42
43 23 wake interferences during VIM. The accuracy and reliability of the current numerical approach is
44
45 24 assessed.
46
47
48
49
50
51 25 **Keywords:** Vortex-induced motions; paired-column semi-submersible; detached-eddy
52
53
54
55
56
57
58

simulation; overset grid; naoe-FOAM-SJTU solver

27

1. Introduction

Modern offshore structures are often designed to have deep draft stabilized columns and low gravitational center in order to suppress the wave-induced motions, especially for heave motions.

These column structures are subject to motions that are induced by the periodical fluctuation forces and vortex shedding when currents velocities exceed a few knots. The term vortex-induced

motions (VIM) is coined to describe the phenomenon as the motions are caused by vortices. VIM is a matter of high complexity, mainly due to the high Reynolds numbers turbulent flows around

floating structure with complex geometry, as well as six-degrees-of-freedom motions that are determined by various kinds of forces such as hydrodynamic forces, mooring forces, gravitational

forces, not to mention the interaction between the fluids and structures. VIM is similar to vortex-induced vibrations (VIV). The latter generally represents the high frequency vibrations of

rigid or flexible cylinders with large aspect ratio, such as risers and cables. In contrast, VIM describes the much longer period motions of large volume offshore structures, such as Spars,

monocolumn, semi-submersibles, TLPs and buoys. In the oil drilling production environment, the floating structures are moored with mooring lines. The floating structure and mooring lines can be

treated as a spring-mass system. When the frequency of external excitation (vortex shedding or transverse hydrodynamic force) is at or near the structural natural frequency of the system in still

water, the storage of vibrational energy increases rapidly which produces large amplitude oscillations up to one diameter of column. Unlike stationary cylinder whose shedding frequency is

1 47 proportional to velocity, the shedding frequency of spring-supported cylinder is locked in one
2
3 48 natural frequency of the cylinder. This so-called “lock-in” phenomenon greatly accelerates the
4
5
6 49 fatigue failure of mooring and risers system and reduces the service life span of offshore platforms
7
8
9 50 [1].

10
11 51 There have been plenty of studies on VIM for various kinds of offshore platforms, most of which
12
13
14 52 are performed by means of model tests in towing tanks and numerical simulations with
15
16
17 53 computational fluid dynamic (CFD). Geometric similitude is important for model test and is
18
19
20 54 achieved by scaling not only model geometry but also appurtenance from prototype accurately.
21
22
23 55 Another important aspect is dynamic similitude which requires the properly scale of natural
24
25
26 56 periods, mass ratio and reduced velocities [2]. It is well known that it’s impossible to keep both
27
28
29 57 Reynolds number scaling and Froude number scaling for hydrodynamic model testing of offshore
30
31
32 58 structures. VIM model tests apply Froude scaling for hydrodynamic similitude due to the speed
33
34
35 59 limitation of towing facilities. The scaling effect brought by Reynolds number has been addressed
36
37
38
39 60 by Roddier et al. [3]. They conducted a series of model tests for the hard tank part of a Truss Spar
40
41
42 61 model in three different scale ratios (three different Reynolds regimes) and concluded that there
43
44
45 62 are little differences between sub-critical and super-critical regimes, which means Froude scaling
46
47
48 63 in terms of geometric and dynamic similitude is applicable for VIM.

49
50 64 Recently, numerical simulation based on CFD has been improved with the advancing of
51
52
53 65 computer science and numerical modeling. There have been significant progress in the application
54
55
56 66 of CFD to predict deep-draft semi-submersible VIM [4–11]. The comparison of CFD results
57
58
59 67 against model test data in these literatures shows the capability of CFD in modeling VIM with

68 remarkable accuracy. Most of the simulations were carried out with commercial CFD software,
 69 such as the finite element solver AcuSolve [4,7,8,11] and the finite volume solvers Star-CCM+[5,7]
 70 and Fluent [7,8]. Exceptions are Lee et al. [6] and Chen and Chen [9] who investigated the
 71 round-corner effect and scale effect of VIM of a deep-draft semi-submersible at model scale and
 72 full scale using an in-house Finite-Analytic Navier-Stokes (FANS) code which solves
 73 Reynolds-Average Navier-Stokes (RANS) equations in curvilinear body-fitted coordinate system
 74 with overset structured grid capability. Rosetti et al. [12] presented numerical simulations of VIM
 75 of a semi-submersible with circular columns in 0 and 45 degrees current heading by using
 76 ReFresco which is an in-house viscous-flow CFD code that solves multiphase unsteady
 77 incompressible flows using Navier-Stokes equations. Recently, the open source CFD software
 78 OpenFOAM raises as a popular CFD software in both academia and industry due to its flexible
 79 and extensible design and good source code quality. It's easy and convenient to implement
 80 customized functionality based on the framework. Zhao et al. [13] simulated VIM of a Spar
 81 platform in uniform currents using an in-house solver naoe-FOAM-SJTU which is developed
 82 based on OpenFOAM. The effectiveness of helical strake on suppressing VIM was discussed.
 83 Kara et al. [10] calculated VIM of a paired-column semi-submersible using the free, open source
 84 CFD software OpenFOAM. They implemented an in-house 6 degree-of-freedom (6DoF) solver
 85 with nonlinear coupling of accelerations and velocities to solve the motions. The 6DoF solver has
 86 an interface for generalized external forces such as spring forces. They also highlighted the key
 87 aspects of CFD methodology for VIM simulations and concluded that the detached-eddy
 88 simulation (DES) is a powerful turbulence model in estimating response amplitude and periods.

1 89 In the present paper, the CFD simulation of a paired-column semi-submersible with eight-columns
2
3 90 and squared-pontoon hull configuration is performed using the in-house CFD code
4
5
6 91 naoe-FOAM-SJTU. To resolve the turbulent wake structures and predict the wake interference
7
8
9 92 between columns and pontoons, a DES turbulence model (SST-DDES) is employed. An
10
11
12 93 unstructured overset grid approach is adopted to avoid mesh distortion and support the arbitrary
13
14
15 94 large movements of hull. The objective of the present study is to demonstrate the validity of the
16
17
18 95 current numerical approach to VIM problems. The approach is discussed and applied to a problem
19
20
21 96 of VIM for semi-submersibles. Results are compared with experiments and simulation results
22
23
24 97 from the RPSEA 5404 project [14].

25 98 **2. Mathematical and numerical methods**

26
27
28 99 A finite volume CFD solver naoe-FOAM-SJTU [15,16] is used to perform all simulations. The
29
30
31 100 naoe-FOAM-SJTU was initially developed based on the open source platform OpenFOAM
32
33
34 101 version 2.0.1. It was derived from *interDyMFoam* (a standard solver from OpenFOAM) with an
35
36
37 102 in-house 6DoF solver based on Euler angles and a wave generation and absorption module for
38
39
40 103 various types of regular and irregular waves common in marine and ocean engineering.
41
42
43 104 Furthermore, the dynamic overset capability was implemented into the solver in coupled with
44
45
46 105 Suggar [17] to perform large amplitude hull motions. Recently, the solver was upgraded to
47
48
49 106 OpenFOAM version 3.0 and use Suggar++ [18], an improved version of Suggar, to compute
50
51
52 107 domain connectivity information (DCI), and to connect fields solutions among multiple overset
53
54
55 108 mesh blocks. The naoe-FOAM-SJTU has been validated against a majority of steady and unsteady
56
57
58 109 problems [19–21]. In this study, the free surface was neglected due to the low Froude number

condition.

2.1 Governing equations and turbulence modeling

The flow is treated as single-phase and incompressible. The continuity and momentum equations for turbulent flow in vectorial form are written as

$$\nabla \cdot \mathbf{U} = 0 \quad (1)$$

$$\frac{\partial \mathbf{U}}{\partial t} + \nabla \cdot (\mathbf{U} - \mathbf{U}_g) \mathbf{U} = -\frac{1}{\rho} \nabla p + \nabla \cdot (\nu_{eff} \nabla \mathbf{U}) + (\nabla \mathbf{U}) \cdot \nabla \nu_{eff} \quad (2)$$

where, \mathbf{U} is the fluid velocity and \mathbf{U}_g is the grid velocity, p is the pressure and ρ is the fluid density. The effective viscosity is defined as $\nu_{eff} = \nu + \nu_t$, where ν is the molecular viscosity and ν_t is the turbulent eddy viscosity.

The delayed DES (DDES) formulation of $k-\omega$ shear stress transport (SST) model is employed for turbulence modeling. The SST model is a blended $k-\omega/k-\varepsilon$ model which has been proven to be robust and accurate for turbulent flows around complex geometries in industry. DDES is a hybrid RANS/LES method which combines the best practice of RANS and LES in a single solution strategy. In this study, SST-DDES solves flow field using $k-\omega$ SST model in the near wall regions and converts to LES subgrid-scale model in other regions after flow separation. The transport equations for SST are given as

$$\frac{\partial k}{\partial t} + \nabla \cdot (\mathbf{U}k) = \tilde{G} - \frac{k^{3/2}}{l} + \nabla \cdot [(\nu + \alpha_k \nu_t) \nabla k] \quad (3)$$

$$\frac{\partial \omega}{\partial t} + \nabla \cdot (\mathbf{U}\omega) = \gamma S^2 - \beta \omega^2 + \nabla \cdot [(\nu + \alpha_\omega \nu_t) \nabla \omega] + (1 - F_1) CD_{k\omega} \quad (4)$$

where k is the turbulent kinetic energy and ω is the specific dissipation rate. The turbulence length scale l in SST model is defined as $l = l_{RANS} = \frac{k^{3/2}}{\beta^* k \omega}$. SST-DDES modifies the length scale to become l_{DDES} which can be written as

$$l_{DDES} = l_{RANS} - f_d \max(0, l_{RANS} - C_{DES} \Delta) \quad (5)$$

where f_d is empiric blending function defined as

$$f_d = 1 - \tanh \left[(C_{d1} r_d)^{C_{d2}} \right] \quad (6)$$

$$r_d = \frac{\nu_t + \nu}{\kappa^2 d_w^2 \sqrt{0.5(S^2 + \Omega^2)}} \quad (7)$$

Here S and Ω are strain rate and vorticity tensor invariants, $\kappa = 0.41$ is the von Karman constant, d_w is wall distance. The blending function f_d is zero inside boundary layer to deactivate the DES limiter and protect the boundary layer from earlier separation.

2.2 6DoF rigid body solver

There has already been a standard 6DoF rigid body motion solver in OpenFOAM. In this 6DoF solver, the rigid body motion state is described by quaternions. While in the marine and ocean engineering context, an Euler angle description of motions for marine structures is preferred for convenience. Therefore, an in-house 6DoF solver based on Euler angles for marine hydrodynamic applications was adopted in naoe-FOAM-SJTU [15]. Two coordinates, namely inertia and non-inertia frame, are used for solving the motion equations of the rigid body. The inertial frame or Earth frame is fixed to Earth or moves at a constant speed with respect to the Earth. The non-inertial frame or body-fixed frame is fixed on the rigid body and translates and rotates according to the motions of rigid body with respect to the inertial system. The two coordinate frames are related to each other by the positions (x, y, z) (surge, sway, heave) and Euler angles (ϕ, θ, ψ) (roll, pitch, yaw) of the rigid body in Earth frame. The transformation of linear velocity (u, v, w) angular velocity (p, q, r) in body-fixed frame between the two coordinate frames can be done by two transform matrix J_1 and J_2 [16]. The 6DoF rigid body motion are obtained by

applying Newton's 2nd law and governed by the following equations in body-fixed coordinate frame

$$\begin{cases}
 \dot{u} = X / m + vr - wq + x_g(q^2 + r^2) - y_g(pq - \dot{r}) - z_g(pr + \dot{q}) \\
 \dot{v} = Y / m + wp - ur + y_g(r^2 + p^2) - z_g(qr - \dot{p}) - x_g(qp + \dot{r}) \\
 \dot{w} = Z / m + uq - vp + z_g(p^2 + q^2) - x_g(rp - \dot{q}) - y_g(rq + \dot{p}) \\
 \dot{p} = \frac{1}{I_x} \{ K - (I_z - I_y)qr - m[y_g(\dot{w} - uq + vp) - z_g(\dot{v} - wp + ur)] \} \\
 \dot{q} = \frac{1}{I_y} \{ M - (I_x - I_z)rp - m[z_g(\dot{u} - vr + wq) - x_g(\dot{w} - uq + vp)] \} \\
 \dot{r} = \frac{1}{I_z} \{ N - (I_y - I_x)pq - m[x_g(\dot{v} - wp + ur) - y_g(\dot{u} - vr + wq)] \}
 \end{cases} \quad (8)$$

where m is the mass and I_x, I_y, I_z are the moments of inertia around centre of rotation, X, Y, Z, K, M and N are surge, sway, heave forces and roll, pitch, and yaw moments. By solving the 6DoF motion equations, the linear and angular accelerations in body-fixed frame are obtained. The linear and angular velocities in body-fixed frame are obtained by integral acceleration over time and then they are transformed to Earth system. Finally, the translations and rotations increments are obtained by integral velocities over time and they are used in the next stage for grid motion. The current implementation of 6DoF motion solver reserves an interface of generalized external forces (such as mooring forces or constant force).

2.3 Mooring system

Mooring system consists of several mooring lines. Each mooring line is anchored to a fixed point at one end and attached to the moving body at the other end. The framework of mooring system follows the object-oriented (OO) design approach and OpenFOAM data structures. An abstract base class named *mooringLine* is designed for describing general mooring line. This class provides interfaces such as computing forces and moments (around centre of rotation), updating mooring line shapes. These member functions will be implemented in derived classes for different

types of mooring lines. Currently supported mooring line types include *linearSpring*, *catenary*, *PEM* (piecewise extrapolation method) and *LMM* (lumped mass method). It is easy to extend the mooring system and add new mooring line types based on the current framework thanks to the OO design. Finally, a wrapper *PtrList<mooringLine>* is used for the whole mooring system that consisting all kinds of mooring lines, as shown in Figure 1. The solution procedure of mooring system is as summarized follows: compute mooring forces and moments and add them as external excitation to the rigid body motion equations; solve the 6DoF motion equations and update motion state for rigid body; update the mooring line shape for current time step and step forward to next time step. In the present study, all mooring lines are treated as linear springs.

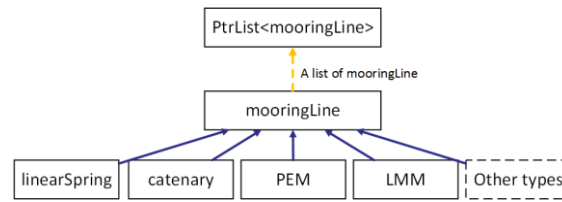


Figure 1: Framework of mooring system module

2.4 Overset grid

The naoe-FOAM-SJTU uses an overset grid system to solve the flow field. This is achieved by the combination of the grid assembly Suggar++ [18] and OpenFOAM. Details of the coupling strategy can be referred to Shen's work [16] and only a brief introduction is presented here.

A parallel scheme is archived in naoe-FOAM-SJTU by running OpenFOAM and Suggar++ processors simultaneously. Suggar++ is responsible for computing DCIs that contain cell type information (e.g., active, hole, orphan, fringe and donor) and interpolating weighting factors. OpenFOAM was responsible for solving fluid, computing forces and motions of the rigid body, updating mesh. DCIs are sent from Suggar++ to OpenFOAM processors with MPI. Currently,

Suggar++ does not recognize OpenFOAM mesh format, a copy of overset mesh will be converted from OpenFOAM format to Suggar++ supported format before computation. In other words, the solver keeps two separated grid instance, one for OpenFOAM and one for Suggar++. The Suggar++ grid is updated with the rigid body motion state obtained by OpenFOAM.

2.5 Solution strategy

The overall solution strategy is illustrated in Figure 2. At the beginning of simulation, OpenFOAM read meshes, boundary conditions and initial conditions for initialization. After that OpenFOAM receives DCIs from Suggar++, performs PIMPLE loop to obtain pressure and velocity and solves transport equations for turbulence quantities. Then pressure, viscous and mooring forces are computed and motions are predicted. The motion data will be sent to Suggar++ to update grids used by Suggar++. The DCIs in Suggar++ processor is decomposed by OpenFOAM's domain decomposition and cell distribution information and will be sent to each OpenFOAM processor.

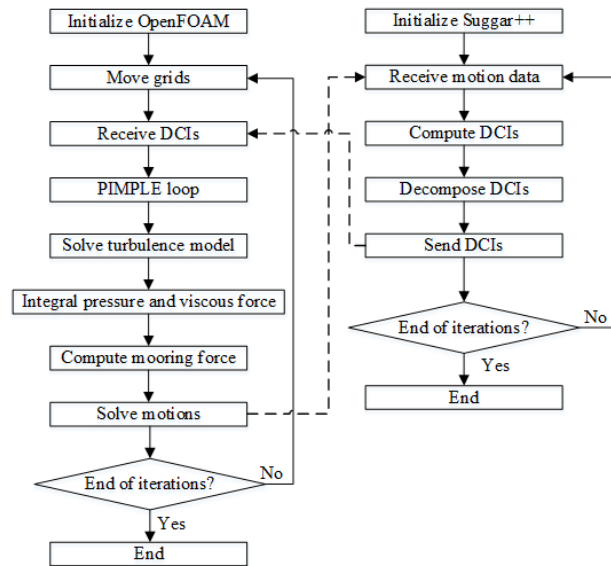


Figure 2: Flow chart of the whole solution strategy

3. Simulation design

3.1 Geometry and conditions

The geometry is a paired-column semi-submersible, which is a part of the RPSEA 5404 project [14]. Figure 3 shows the dimensions of prototype in side view and top view. The column height and pontoon height are 74.4m and 8.2m, respectively, resulting in an overall height of 82.6m. The draft is 53.3m. Columns are divided into outer column (OC) and inner column (IC). OCs are connected to ICs at four corners via pontoon. Both OC and IC have rectangular section, while sizes are different, i.e., 14x13.4m and 14x10.4m, respectively. The base gap between OC and IC is 20.4m, and tensioner stroke is 8.5m. The model scale for PC Semi in the current study is 1:54. Details about the main particular of the PC Semi geometry in both full-scale and model-scale can be found in Table 1.

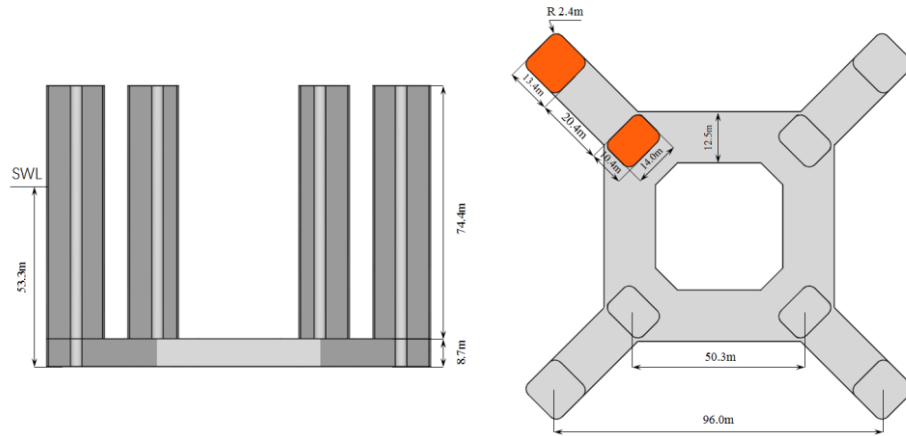


Figure 3: Side view and top view of the prototype geometry

Table 1: Main particulars of the prototype and model

| Name | Notation (unit) | Prototype | Model |
|---------------|-----------------|-----------|-------|
| Overall width | B (m) | 113.4 | 2.1 |
| Draft | T (m) | 53.3 | 0.987 |

| | | | |
|---|----------------------------|------------------|----------------------|
| Immersed column height above pontoon | H (m) | 44.6 | 0.826 |
| Outer column size | $L_{OC} \times W_{OC}$ (m) | 13.4×14 | 0.248×0.259 |
| Outer column characteristic length | D (m) | 19.4 | 0.36 |
| Inner column size | $L_{IC} \times W_{IC}$ (m) | 10.4×14 | 0.192×0.259 |
| Inner column characteristic length | d (m) | 17.4 | 0.32 |
| Center-to-center distance of outer column | S_{OC} (m) | 96.0 | 1.78 |
| Center-to-center distance of inner column | S_{IC} (m) | 50.3 | 0.93 |
| Pontoon height | P (m) | 8.7 | 0.16 |
| Pontoon width | L_p (m) | 12.5 | 0.23 |

The case conditions consist of two parts: the stationary drag and the VIM simulation. In stationary drag simulation, the semi-submersible is fixed and not allowed to move. Static overset grid is used for stationary drag simulation. In this approach, as the hull is stationary and grids do not move, DCIs are computed at the beginning of the simulation and do not need to be updated in the following time steps. VIM simulation utilizes dynamic overset grid to perform hull boundary movement. In every time step, the DCIs are reinitialized automatically to update the hole-cutting geometry. Motions in horizontal plane (e.g., surge, sway and yaw) are allowed during VIM

simulation.

3.2 Coordinate system and grids

A right-handed Cartesian coordinate system O -XYZ is used in the simulations. The origin O is located at the center point of hull geometry on the surface water line. X -axis coincides with current direction and points towards the downstream. Y -axis points to the transverse direction (starboard) that perpendicular to current and Z -axis points upwards.

The computational domain is set as $7B \times 4B \times 3.5T$ (length \times width \times depth) for all simulations as shown in Figure 4. Here, B is the overall width and T is the draft of the hull. In previous studies of semi-submersible VIM, the computational domain size are slightly different. Kim et al. [4] used a domain of $14B \times 12B \times 4.5T$. A $27B \times 18B \times 6T$ domain was adopted by Tan et al. [5], and $18B \times 12B \times 6T$ by Liu et al. [22]. Compared with these domains, smaller domain size is also acceptable. For example, Lee et al. [6] numerically studied VIM of a deep-draft semi-submersible using computational domains of $6B \times 4.5B \times 2.8T$ and $5B \times 4B \times 2.2T$. A $9B \times 6B \times 3T$ domain was selected by Liang and Tao [23] in their studies of vortex shedding process of flow around a deep-draft semi-submersible. It is reasonable that the current domain size is large enough to eliminate effect from boundaries at two lateral sides, downstream and bottom.

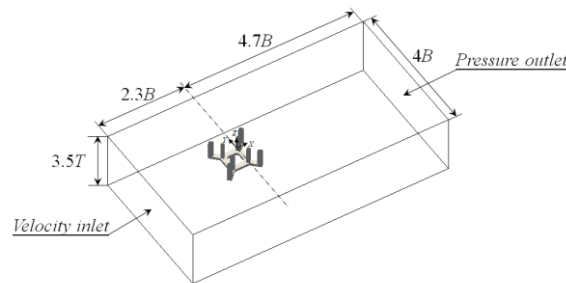


Figure 4: Computational domain and boundaries

A constant and uniform flow condition is employed for all simulations. The boundary condition for velocity is set as $(U, 0, 0)$ (U the current velocity) at inlet and zero gradient at outlet. As for pressure, a zero gradient boundary condition and zero value is set for inlet and outlet, respectively. Symmetry planes are specified for two lateral sides and bottom boundaries. Besides, symmetric boundary condition is also applied for top due to the ignorance of free surface effect at low Froude number conditions. For hull surface of the PC Semi, a no-slip boundary condition is prescribed which assigns the velocity to U_{wall} and the pressure to zero normal gradient. An unstructured polyhedral multi-block overset grid system is used throughout the present study. The grid system consists of two blocks, namely the background and hull grid, which are generated individually and then assembled into a single mesh. The background mesh block is hexahedral and has a uniform grid spacing. The hull mesh block is based on predominantly Cartesian cut-cell approach and has a same initial base grid size with background mesh block to avoid orphans when performing overset DCI calculation. The near hull and wake regions are refined in the hull mesh block in order to capture the boundary layers and wake structures induced by flow separations. Four different levels of refinement zones are utilized to archive higher accuracy in critical regions. In the vicinity of columns and pontoons, 10 prism cell layers are applied to hull boundary to capture the boundary layer development. For all cases, the non-dimensioned wall distance of the first layer satisfies $y^+ < 1$, which makes sure the first layer cells are located in the viscous sublayer. An example mesh can be found in Figure 5.

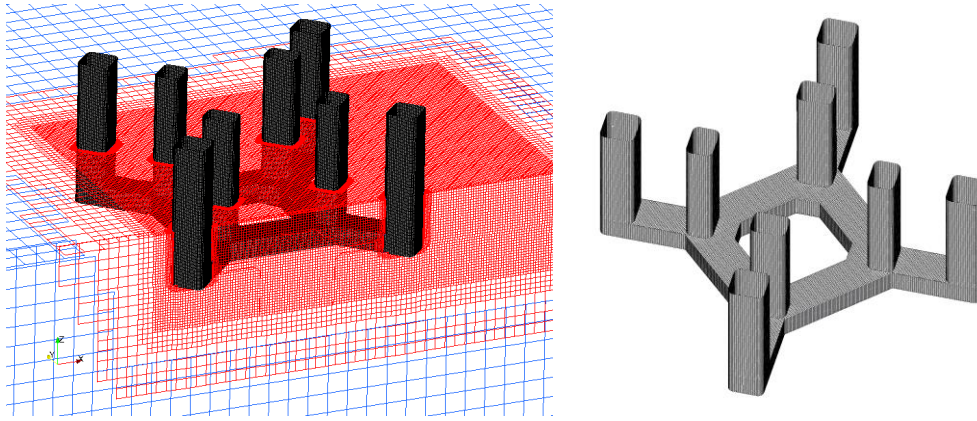


Figure 6: Overset mesh assembly and hull surface mesh

DES resolves scales in the wake regions after flow separation. Thus, it is vital to avoid excessive numerical dissipation, which is guaranteed by discretizing all terms in governing equations using high-order schemes. The temporal derivatives in both momentum and turbulence quantities equations are discretized by second-order backward differencing scheme. A second-order upwind scheme, stabilized for transport (linear-upwind stabilized transport, LUST) is applied for convection term in momentum equation. For turbulent quantities convection terms, a second-order Total Variation Diminishing (TVD) limited linear scheme is used. The merged PISO-SIMPLE (PIMPLE) algorithm is used for pressure-velocity decoupling.

3.3 Mooring stiffness

The most vital part of mooring system is not the configuration of the mooring lines but the equivalent restore stiffness provided by the mooring system. As the stiffness has direct influence on the moored floating body's natural period which significantly affect the VIM response characteristics. To make the comparison with experimental data meaningful, one must verify the effective stiffness before VIM simulation. In the experiments [24], the model was equipped with frictionless air bearings that slide along a horizontal plate. This air bearing system allows the

model moving freely in the horizontal plane. Meanwhile, the vertical motions are constrained.

Table 2 lists the mass and stiffness properties of the hull and mooring system from experiment.

Table 2: Main particular for mass and stiffness system at model scale

| Name | Value | Dimensions |
|---------------------------|---------|------------|
| Mass | 490.2 | kg |
| Radius of gyration | 0.77593 | m |
| Transverse stiffness | 173.98 | N/m |
| Yaw stiffness | 5.23 | Nm/deg |
| Transverse natural period | 15.45 | s |
| Yaw natural period | 9.32 | s |

In the present numerical simulations, an equivalent horizontal mooring system is used. The mooring system consists of four linear springs that distribute along positive and negative X -axis and Y -axis. Figure 7 depicts the sketch of the mooring system. All spring are pretensioned and the pretension should be large enough to ensure that the spring would not relax during VIM.

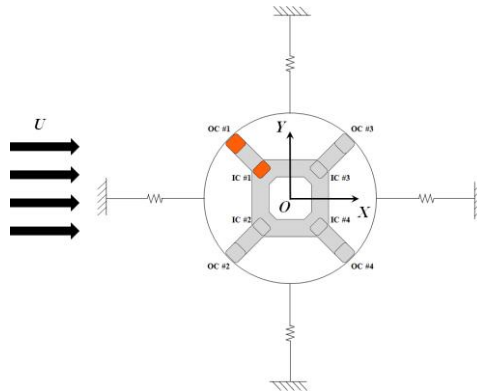


Figure 7: Schematic of the mooring system configuration

To perform validation for stiffness, static offset tests and free decay tests are carried out in sequence. In static offset tests, the hull is prescribed to move in Y -axis and rotate around Z -axis, respectively, without solving flow field. Parameters such as stiffness and pretension of each spring are adjusted to match the global horizontal and vertical (yaw) stiffness of model test. After static offset test, the spring parameters are used for free decay tests. The free-decay tests allow hull oscillating with a prescribed initial offset or velocity in the absence of inflow. Transverse and yaw decay test are conducted separately to verify the natural transverse and yaw period of the mooring system. The time histories and spectral analyses of free decay test are shown in Figure 8. The deviations of natural period between CFD and EFD for transverse motion and yaw are 0.6% and 2%, respectively, showing the correct equivalent linear and rotational stiffness are provided by the current mooring configuration.

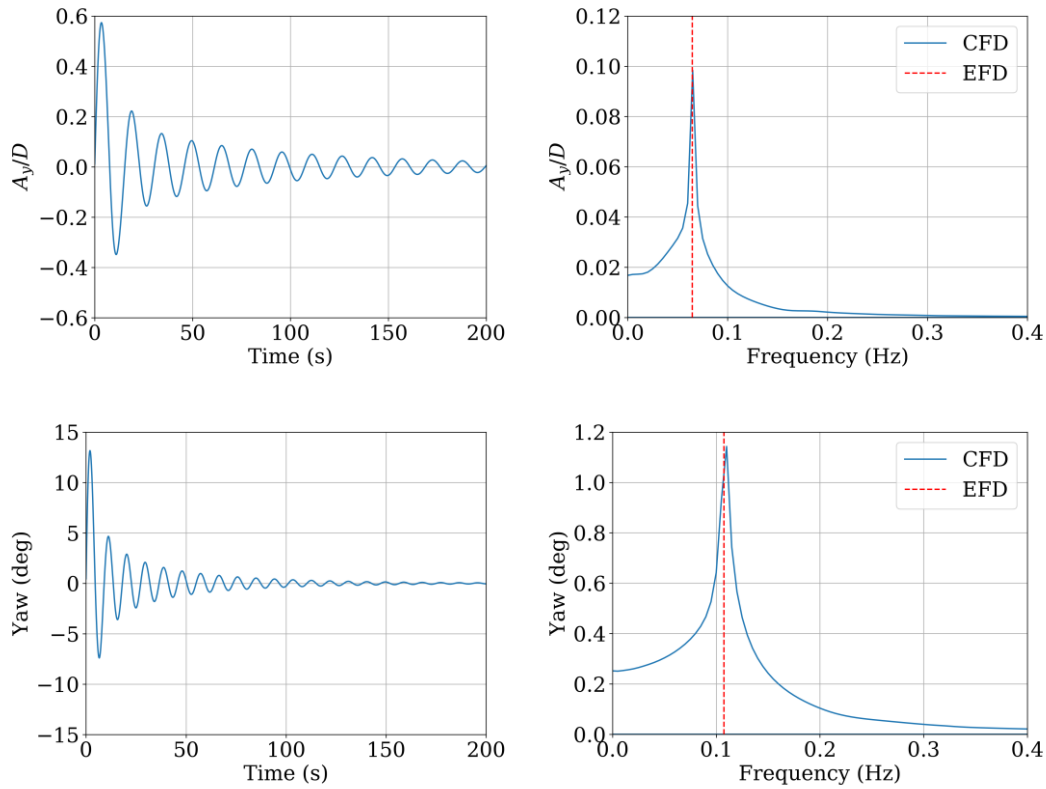


Figure 8: Time history and spectral analysis of transverse and yaw decay test

4. Results and discussion

4.1 Stationary drag simulation

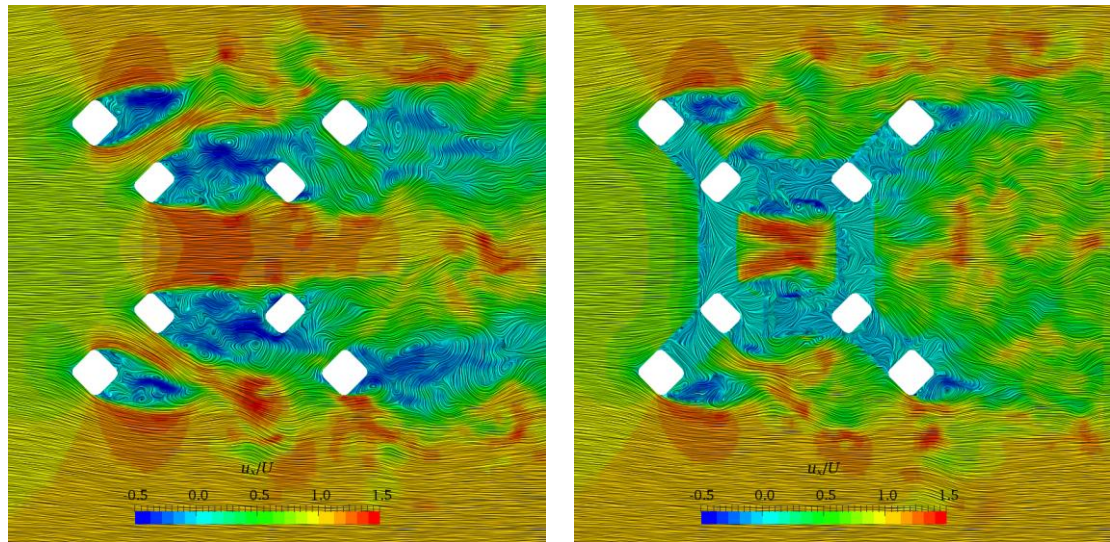
In this case, the current velocity is 0.272m/s. The time step is set to 0.02s in all simulations including VIM simulations in the next section. Grid convergence study is performed on this case. Three different mesh sizes are considered. Note that the overset mesh blocks used in the current study is unstructured grid. The background mesh block is uniform hexahedral mesh and is easy to refine in three directions of the Cartesian coordinate system. Contrary to background, the hull mesh block is obtained by cut and splitting cells in refinement region on an initial Cartesian grid. Following the recommendation by Shen et al. [15,16], to achieve consistent grid refinement ratio in three directions, the Cartesian grid is refined systematically by a factor. Table 3 lists the details of different cases in grid sensitivity study. Grid refinement ratio $r=1.4$ is selected for convergence study. Total grid number for coarse, medium and fine mesh are 1.04×10^6 , 2.53×10^6 and 6.25×10^6 , respectively. The grid independent study shows that S_2 is fine enough to get reliable results at a relatively low computational cost and it is used in the following studies.

Table 3 Grid independent study for stationary drag simulation

| Case | ID | No. of cells ($\times 10^6$) | | | $\overline{C_D}$ | C_{Lrms} |
|--------|-------|--------------------------------|------------|------|------------------|------------|
| | | Total | Background | Hull | | |
| Fine | S_1 | 6.25 | 0.29 | 5.96 | 0.673 | 0.021 |
| Medium | S_2 | 2.53 | 0.10 | 2.43 | 0.689 | 0.022 |
| Coarse | S_3 | 1.04 | 0.04 | 1.00 | 0.726 | 0.048 |

| | | | | | |
|-----|---|---|---|----------------------|---|
| EFD | - | - | - | 0.683($\pm 3.0\%$) | - |
|-----|---|---|---|----------------------|---|

Figure 9 shows the instantaneous flow visualizations presented by streamwise velocity contour and streamlines on two cut-planes at $z/H=-0.5$ and $z/H=-1$. It can be seen that wake interference between side-by-side OCs is insignificant. However, the wake behind front OC is strongly influenced by the front IC. Asymmetric wake is observed due to the speed up between front OC and IC. The wake interaction between front and rear ICs is clear due to the small spacing ratio ($L/d=2.89$). As for front and rear OCs, the spacing ratio ($L/D=4.95$) is large enough that the wake interference is trivial. Figure 9(b) shows the existence of pontoon suppresses vortex sheds from the front OC inner flank. The coherent vortical structures along column vertical direction is destroyed at the low end by pontoon. This may indicates the damp effect of pontoon on VIM behavior.



(a) $z/H=-0.5$ (b) $z/H=-1$

Figure 9: Instantaneous streamwise velocity contours and streamlines

4.2 VIM simulation

The non-dimensioned parameter reduced velocity is crucial to VIM response. It is defined as

$$U_r = \frac{UT_n}{D} \quad (9)$$

where U is the current velocity or towing velocity, T_n is the natural transverse period in still water and D is the characteristic length of the platform. In previous studies of semi-submersible VIM, see for example [25–27], D was the projected length of column section perpendicular to flow direction. While in the current study, D is 0.36m, which is the diagonal length of OC's cross section. The definition is consistent with model test.

Five reduced velocities are considered. The model-scale current speeds range from 0.07m/s to 0.26m/s. The corresponding Reynolds numbers are in the order of 10^4 . When discussing motion characteristics of VIM, two sets of non-dimensional nominal responses are used throughout the present study. One is based on the root mean square [28,7,24] and the other is based on standard deviation [25] of motion response time series. The corresponding definitions are listed below

$$(A_x / D)_{rms} = \frac{\sqrt{2}RMS(A_x(t))}{D}, (A_y / D)_{rms} = \frac{\sqrt{2}RMS(A_y(t))}{D}, (Yaw)_{rms} = \sqrt{2}RMS(yaw(t)) \quad (10)$$

$$(A_x / D)_{std} = \frac{\sqrt{2}\sigma(A_x(t))}{D}, (A_y / D)_{std} = \frac{\sqrt{2}\sigma(A_y(t))}{D}, (Yaw)_{std} = \sqrt{2}\sigma(yaw(t)) \quad (11)$$

Where RMS and σ are the root mean square and standard deviation from motion time series, respectively, $A_x(t)$, $A_y(t)$ and $yaw(t)$ are time histories for in-line, transverse and yaw motions, respectively. To better representing the VIM characteristics, the transition stage at the beginning of VIM response is eliminated for all simulations when performing statistical analysis and spectral analysis.

The nominal response in transverse direction is plotted in Figure 10. The black hollow square and circle represent the experimental data and CFD results taken from [24]. It's worth noting that the

results at $U_r=5$ from model test have large dispersion for three repeated runs. In CFD simulations, it takes longer time (40 dimensionless time step) for this particular case to reach pseudo steady state (quasi-sinusoidal transverse motion). This can be interpreted as the beginning of lock-in range. The vibrational energy stored in the system is increasing slowly at this condition. This was also found by Chen and Chen [9] in their CFD simulations of a deep draft semi-submersible. They stated that for a rounded-corner column semi-submersible at $U_r=6$ for model scale and at $U_r=4.4$ for prototype, a thousand more time steps is needed to reach the nominal amplitudes. As the current velocity increases, the vibrational energy increases more rapidly and the time to reach nominal amplitude decreases. The discrepancies between present CFD and AcuSolve is rather small. While both CFD results deviate from EFD with variation no more than 15%. Nevertheless, it is reasonable that the current approach of VIM simulation can be considered reliable.

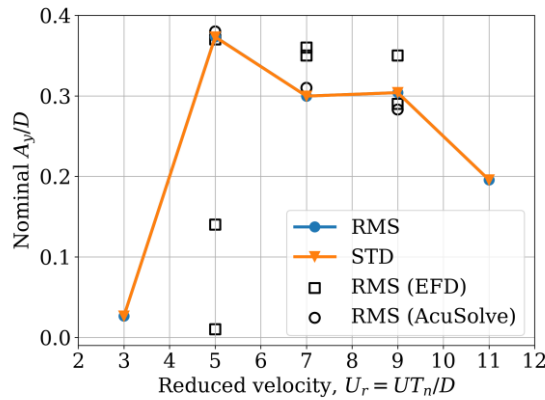


Figure 10: Nominal response of transverse motion

The RMS and STD are complete coincidence, meaning the average position of transverse motion is near 0. When reduced velocity is small ($U_r=3$), the nominal transverse motion response is rather small (about 0.02). As the reduced velocity increases, the nominal response increases promptly, suggesting a synchronized behavior in transverse motions ($5 \leq U_r \leq 9$). The maximum amplitude is

up to 0.37 and occurs at the beginning of lock-in range ($U_r=5$).

Figure 11 shows the nominal response in in-line direction. RMS represents the average offset to origin and STD represents the fluctuation of VIM in in-line direction. For immersed structure exposed to current, the overall drag on structure increases with the current velocity increases. The offset between equilibrium position and origin becomes larger. This explains the increasing RMS of in-line response. Compared with transverse motion, the STD of in-line motion is small, which indicates much smaller fluctuation of in-line response. In addition, larger STD values are found at higher reduced velocities ($9 \leq U_r \leq 11$), which may be caused by the unsteady nature of the force and moment in post-lock-in range.

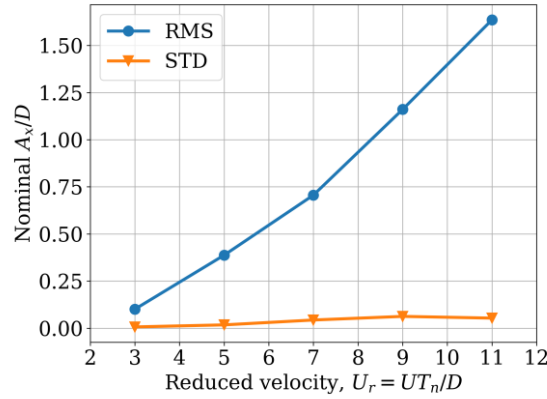


Figure 11: Nominal response of in-line motion

In similar, Figure 12 shows the nominal response of yaw motion. The nominal yaw motion is monotonically increasing and reaches to about 2.55 degree at $U_r=11$. As mentioned previously, the natural yaw period ($T_{n,yaw}=9.32s$) is much smaller than the natural transverse period ($T_n=15.45s$). Obviously, yaw motion has a much higher natural frequency. Amongst the current cases, even the highest reduced velocity does not reach the range which synchronization occurs between vortex shedding and yaw motions. Redefining reduced velocity by yaw natural period $U_{r,yaw} = \frac{UT_{n,yaw}}{D}$,

$U_r=11$ is corresponding to $U_{r,yaw}=6.6$, which is exactly the lock-in range in terms of yaw. We have no reason to doubt that as current velocity continually increasing, the nominal yaw response may still increase but eventually decrease when it comes to the post-lock-in range in terms of yaw.

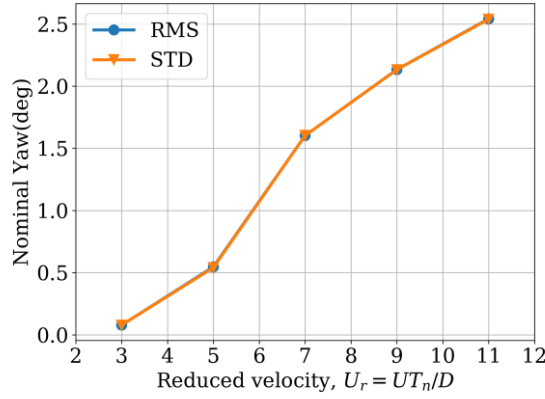
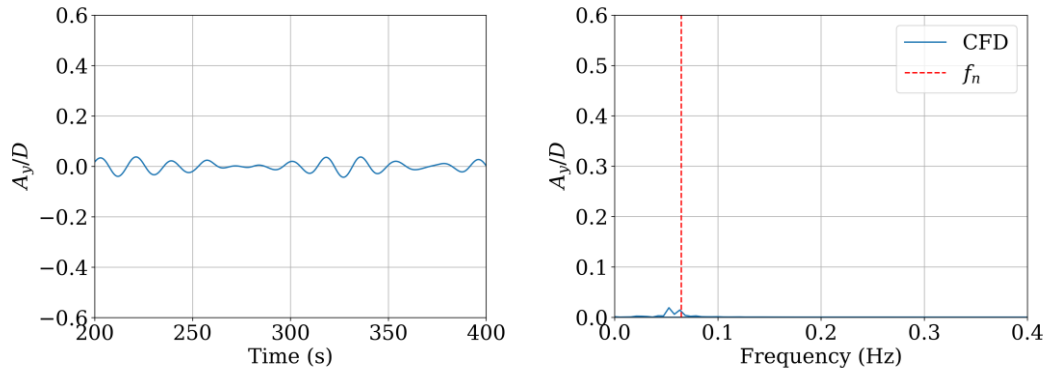
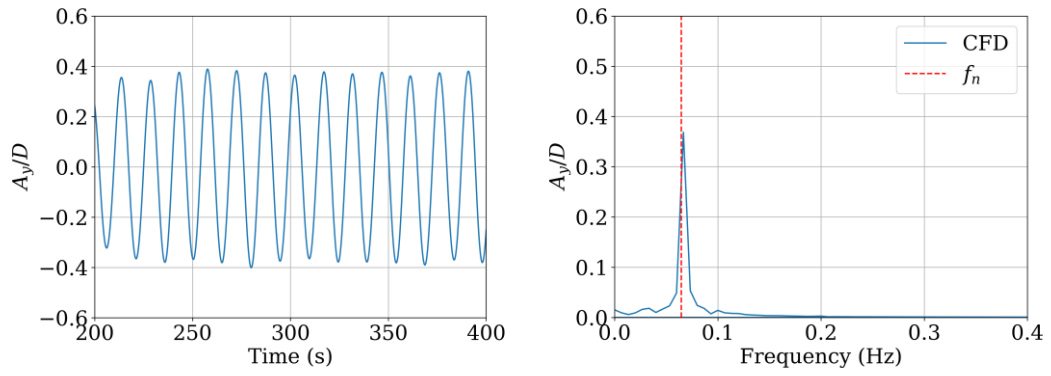


Figure 12: Nominal response of yaw motion

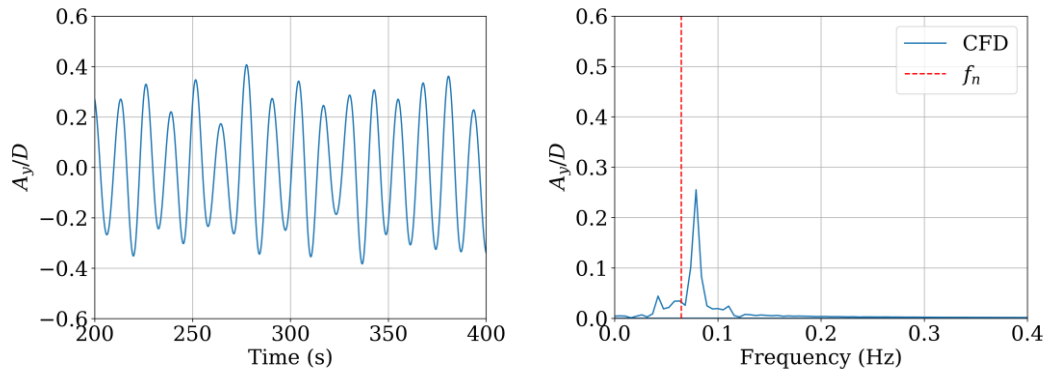
To better understanding the motion characteristics at different reduced velocities, further spectral analysis are performed for transverse, in-line and yaw motions. Figure 13 depicts the time history and FFT spectral analysis results for transverse motion at different reduced velocities. At low reduced velocity ($U_r=3$), the small and irregular motion response with multiple frequencies suggest a motion state before lock-in. After entering lock-in range, the transverse motion is characterized by a dominant frequency which can be clearly seen in Figure 13(b)-(d). This confirms the strong modulated transverse motion in lock-in range. Unlike VIV, in which the shedding frequency is locked on one natural frequency in a wide range of reduced velocities (see for example [29]), the motion frequency of semi-submersible does not lock on one particular frequency. Instead, it increases as the increasing of reduced velocity. This may be attributed to the complex hull geometry (e.g., the multi-column structure and pontoon).



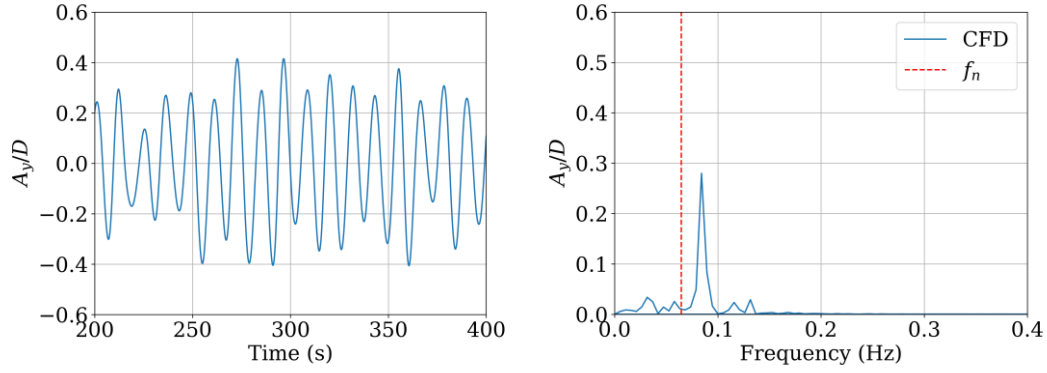
(a) $U_r=3$



(b) $U_r=5$



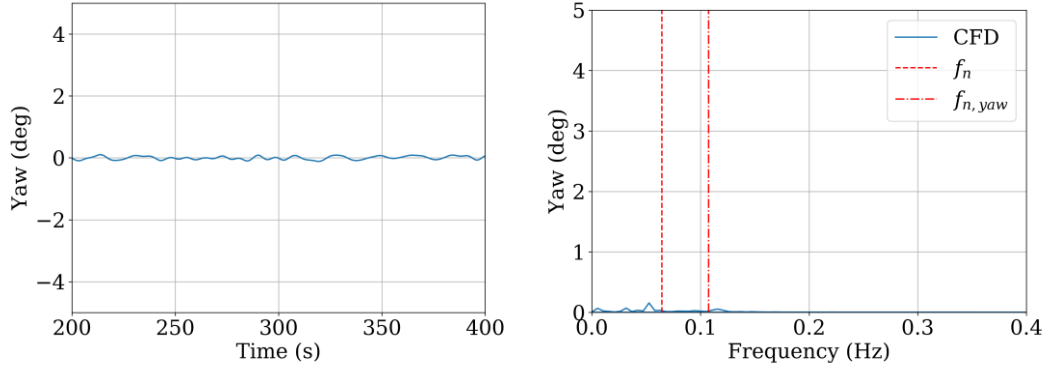
(c) $U_r=7$



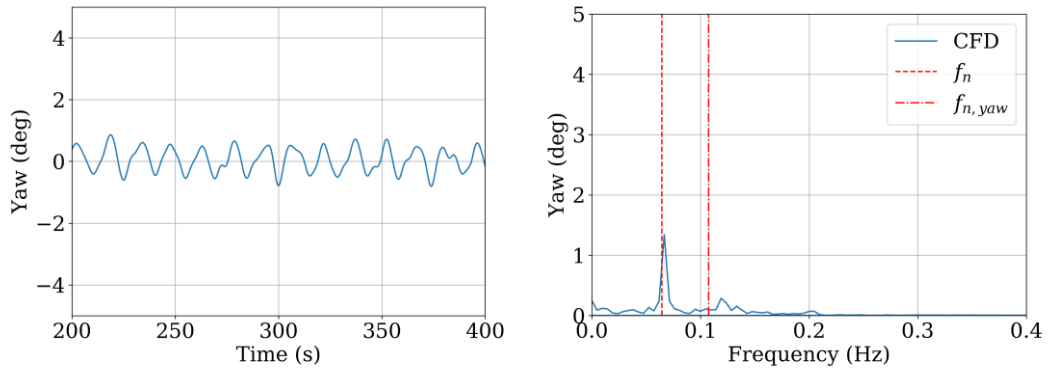
(d) $U_r=9$

Figure 13: Time history and spectral analysis of transverse motion

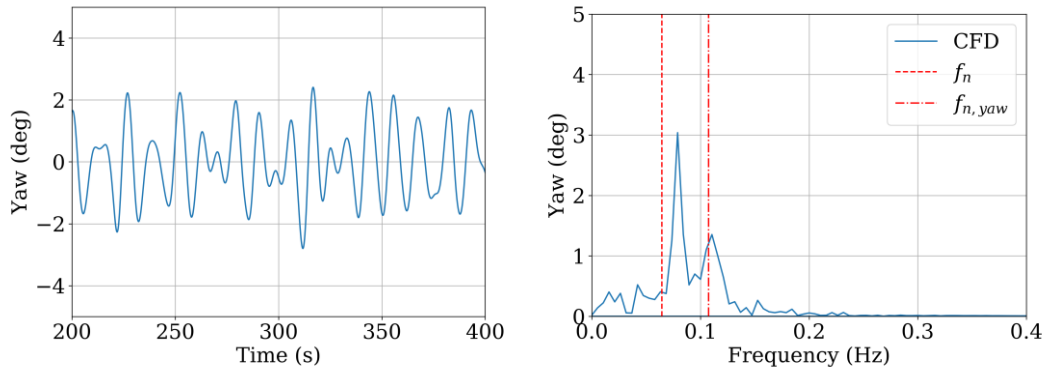
Similar to transverse motion, the time history and FFT spectral analysis for yaw motion are detailed in Figure 14. At pre-lock-in regime (e.g., $U_r=3$), yaw is fluctuating at small amplitude like transverse motion. When entering lock-in range ($U_r=5$), dominant frequency occurs and characterizes the yaw motion. It should be emphasized that as the reduced velocity continually increases, a second dominant frequency appears near yaw natural frequency. The first peak frequency is undoubtedly the consequence of vortex shedding, as it is coincidence with the transverse motion frequency at corresponding velocity. This corroborates that the yaw motion of semi-submersible is induced by vortex shedding. The phenomena was termed vortex-induced yaw or VIY [30]. The occurrence of the second dominant frequency is induced by the interaction, particularly the synchronization between yaw motion and vortex shedding. This was previously reported by Gonçalves et al [30] reported in their model test of a large-volume semi-submersible platform. The existence of VIY shows the importance of yaw motions together with transverse motions in the VIM study of semi-submersibles. It also increases the difficulty and complexity to estimate the fatigue failure of risers and mooring system for semi-submersibles.



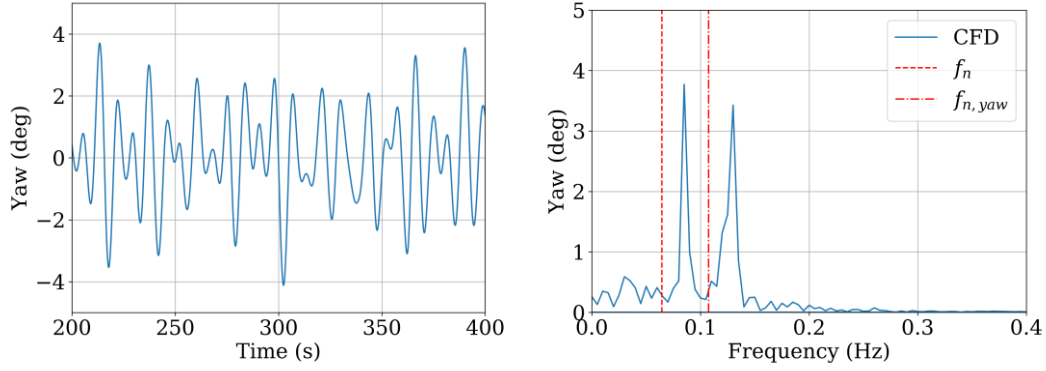
(a) $U_r=3$



(b) $U_r=5$



(c) $U_r=7$



(d) $U_r=9$

Figure 14: Time history and spectral analysis of yaw motion

Figure 15 plots the motion trajectories of the hull centroid on horizontal plane. No typical eight (8) shape trajectory is observed for all conditions. In lock-in range, the synchronized behavior results in pronounced transverse motion amplitude. The transverse motion response in post-lock-in range is the same magnitude to that in lock-in range. However, the in-line response fluctuates much stronger in pre-lock-in range. Trajectories at higher reduced velocities become more erratic.

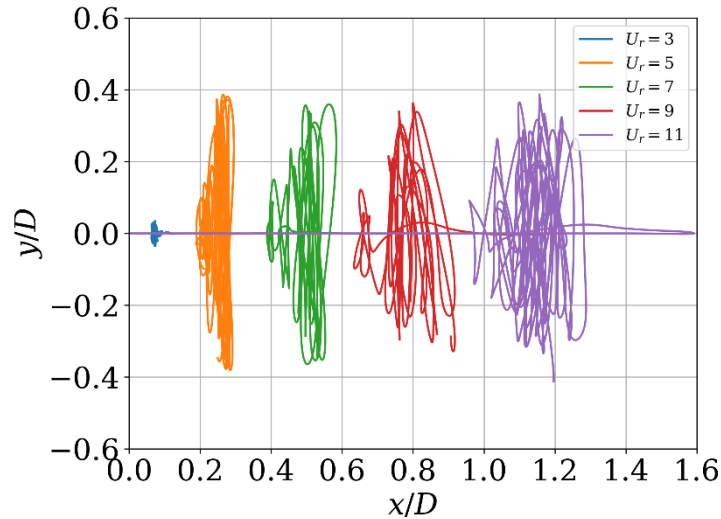


Figure 15: Motion trajectories of centroid at different reduced velocities

To analysis the effect of columns and pontoon on VIM characteristic, the work done by each

component during stabilized VIM are calculated and presented in Figure 16. The work done is calculated with the following formula [31]

$$\begin{aligned} W_x &= \int F_x(t) \cdot \dot{x}(t) dt \\ W_y &= \int F_y(t) \cdot \dot{y}(t) dt \\ W &= W_x + W_y \end{aligned} \quad (12)$$

where W_x and W_y is work done in the in-line and transverse directions, respectively. W is total work done. $F_x(t)$ and $F_y(t)$ are hydrodynamic force on each component in the in-line and transverse directions, respectively.

For convenience, the columns are labeled by numbers. The definition can be found in Figure 7. Overall the work done by pontoon is negative for all reduced velocities. The magnitude of negative work done by pontoon are much larger than a single column, suggesting that pontoon could effectively mitigate VIM response. At low reduced velocity ($U_r=5$), the excitations of VIM are mainly from upstream columns (OC #1 and #2, IC #1 and #2). The downstream OCs damp VIM a little and ICs have nearly no effects on VIM. However, this is not always the case. The work done by two upstream OCs turn from positive to negative at high reduced velocity ($U_r=9$). On the contrary, the work done by other columns except two upstream OCs are all positive. The reason for this change is unclear yet. A possible explanation may be attributed to the complex wake interaction in this unique design of paired-column hull structure, as the work done transition from positive to negative did not observed in previous study of conventional four-column semi-submersibles [23,31].

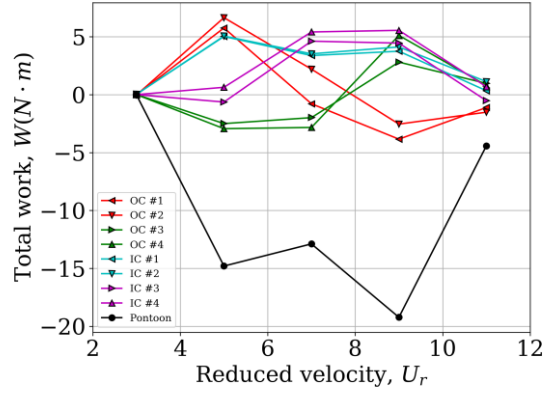


Figure 16: Total work done by each component

Figure 17 presents the instantaneous spanwise vorticity contour at different reduced velocities. The vorticity is non-dimensionalized by the characteristic length and current velocity. The vortex shedding mainly occurs at two lateral rounded corners for each upstream column. Vortices shed from upstream column directly impinge on the downstream column, then collide and interact with the vortices shed from downstream columns. These vortices quickly break into small eddies in the wake region of downstream columns. As U_r increases to 5, VIM is entering lock-in scenario, the vortex shedding patterns changes distinctively. Synchronized vortex shedding patterns are clearly observed amongst the four upstream columns. Moreover, the vortices generated from two lateral rounded corner are reattaching to the backface of each upstream column after flow separation. This dramatically increases the hydrodynamic force and motion amplitude in transverse direction.

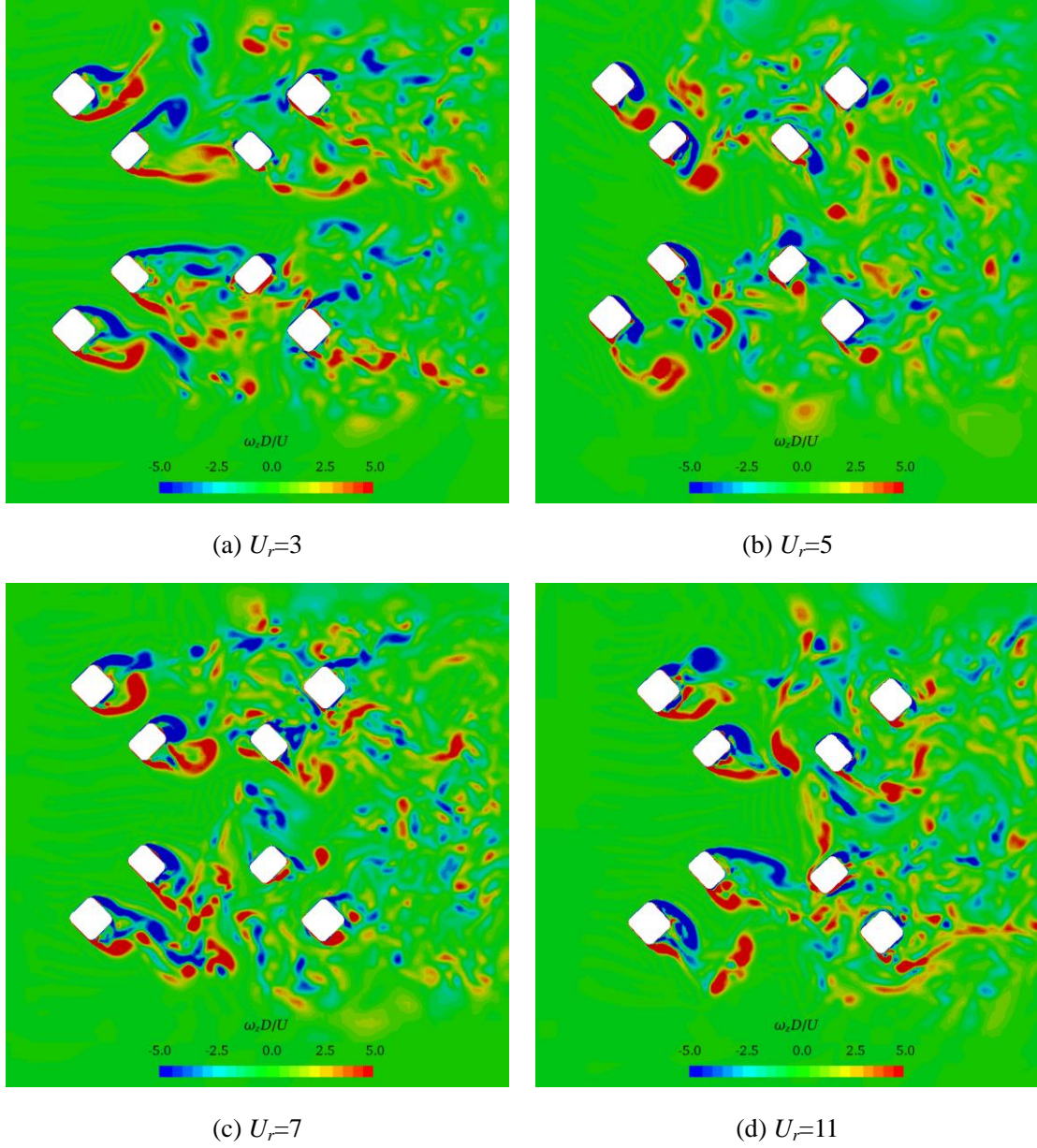


Figure 17: Instantaneous non-dimensional spanwise vorticity contour at half draft ($z/H=-0.5$) plane

5. Conclusions

Stationary drag and VIM simulations of a paired-column semi-submersible at model scale are performed using an in-house CFD solver naoe-FOAM-SJTU. The turbulence flow is modeled with SST-DES method and the motions are obtained by solving 6DoF equations. Dynamic overset grid is used to prevent the near wall mesh distortion during large yaw motions. Results from

stationary drag simulations show that the current DES turbulence is applicable to accurately predict the drag of complex multi-column hull geometry. Several reduced velocities range from 3 to 11 are investigated for VIM. The transverse motion responses predict by the current numerical approach are in good agreement with CFD results by Antony et al. [24]. Spectral analysis using FFT for transverse and yaw motion time series are conducted. The transverse motion in lock-in scenario is governed by dominant frequency equal to vortex shedding frequency. Unlike VIV, the vortex shedding frequency in VIM of semi-submersible does not lock on one natural transverse frequency. It increases as current velocity increases. FFT results for yaw response show that yaw motion is induced by vortex shedding. Synchronized behavior for yaw motion occurs when shedding frequency is approaching yaw natural frequency. The work done by pontoon is always negative, suggesting the damping effect of pontoon on VIM response. The flow reattachment on the backface of upstream columns, together with the synchronized vortex shedding between multiple upstream columns, are accounting for the pronounced VIM motion in lock-in range.

6. Acknowledgement

This work is supported by the National Natural Science Foundation of China (51490675, 11432009, 51579145), Chang Jiang Scholars Program (T2014099), Shanghai Excellent Academic Leaders Program (17XD1402300), Program for Professor of Special Appointment (Eastern Scholar) at Shanghai Institutions of Higher Learning (2013022), Innovative Special Project of Numerical Tank of Ministry of Industry and Information Technology of China (2016-23/09) and Lloyd's Register Foundation for doctoral student, to which the authors are most grateful.

References

- [1] Dijk RRT van, Fourchy P, Voogt A, Mirza S. The effect of mooring system and sheared currents on vortex induced motions of truss Spars. Proc. 22nd Int. Conf. Offshore Mech. Arct. Eng., vol. 1, Cancun, Mexico: 2003, p. 285–92.
- [2] Finnigan T, Roddier D. Spar VIM model tests at supercritical reynolds numbers. Proc. 26th Int. Conf. Offshore Mech. Arct. Eng., vol. 3, San Diego, California, USA: 2007, p. 731–40.
- [3] Roddier D, Finnigan T, Liapis S. Influence of the Reynolds number on spar Vortex Induced Motions (VIM): Multiple scale model test comparisons. Proc. ASME 28th Int. Conf. Ocean Offshore Arct. Eng., vol. 5, Honolulu, Hawaii, USA: 2009, p. 797–806.
- [4] Kim J-W, Magee A, Guan KYH. CFD simulation of flow-induced motions of a multi-column floating platform. Proc. ASME 2011 30th Int. Conf. Ocean Offshore Arct. Eng., vol. 7, Rotterdam, The Netherlands: 2011, p. 319–26.
- [5] Tan JHC, Magee A, Kim JW, Teng YJ, Zukni NA. CFD simulation for vortex induced motions of a multi-column floating platform. Proc. ASME 2013 32nd Int. Conf. Ocean Offshore Arct. Eng., vol. 7, Nantes, France: 2013, p. V007T08A066.
- [6] Lee S-K, Chien H-P, Gu H. CFD Study of Deep Draft SemiSubmersible VIM. Offshore Technol. Conf.-Asia, Kuala Lumpur, Malaysia: Offshore Technology Conference; 2014.
- [7] Antony A, Vinayan V, Halkyard J, Kim S-J, Holmes S, Spornjak D. A CFD based analysis of the Vortex Induced Motion of deep-draft semisubmersibles. Proc. Twenty-Fifth 2015

- Int. Ocean Polar Eng. Conf., Kona, Big Island, Hawaii, USA: 2015, p. 1048–55.
- [8] Kim SJ, Spornjak D, Holmes S, Vinayan V, Antony A. Vortex-Induced Motion of Floating Structures: CFD Sensitivity Considerations of Turbulence Model and Mesh Refinement. Proc. ASME 2015 34th Int. Conf. Ocean Offshore Arct. Eng., vol. 2, St. John's, Newfoundland, Canada: 2015, p. V002T08A057.
- [9] Chen C-R, Chen H-C. Simulation of vortex-induced motions of a deep draft semi-submersible in current. Ocean Eng 2016;118:107–16.
- [10] Kara M, Kaufmann J, Gordon R, Sharma P, Lu J. Application of CFD for Computing VIM of Floating Structures. Offshore Technol. Conf., Houston, Texas, USA: 2016.
- [11] Vinayan V, Antony A, Halkyard J, Kim S-J, Holmes S, Spornjak D. Vortex-induced motion of deep-draft semisubmersibles: A CFD-based parametric study. Proc. ASME 2015 34th Int. Conf. Ocean Offshore Arct. Eng., vol. 2, St. John's, Newfoundland, Canada: 2015, p. V002T08A003.
- [12] Rosetti GF, Gonçalves R, Fajarra ALC, Koop A. CFD calculations of the vortex-induced motions of a circular-column semi-submersible. Proc. ASME 2016 35th Int. Conf. Ocean Offshore Arct. Eng., vol. 2, Busan, Korea: 2016.
- [13] Zhao W, Shen Z, Wan D. Numerical Investigation of the Vortex Induced Motion of SPAR in Uniform Current. Proc. 24th Int. Ocean Polar Eng. Conf., vol. 3, Busan, Korea: ISOPE; 2014, pp. 362–7.
- [14] Gordon R, Mostofi R. ULTRA-DEEPWATER DRY TREE SYSTEM FOR DRILLING AND PRODUCTION IN THE GULF OF MEXICO. Final Technical Report,

1 511 10121-4405-02, RPSEA-Research Partnership to Secure Energy for America, Report;
2
3 512 2014.
4
5
6 513 [15] Shen Z, Wan D. RANS computations of added resistance and motions of a ship in head
7
8
9 514 waves. Int J Offshore Polar Eng 2013; 23: 263–71.
10
11 515 [16] Shen Z, Wan D, Carrica PM. Dynamic overset grids in OpenFOAM with application to
12
13
14 516 KCS self-propulsion and maneuvering. Ocean Eng., 2015; 108: 287–306.
15
16
17 517 [17] Noack RW. SUGGAR: A general capability for moving body overset grid assembly. 17th
18
19
20 518 AIAA Comput. Fluid Dyn. Conf., Toronto, Ontario, Canada: 2005.
21
22
23 519 [18] Noack RW, Boger DA, Kunz RF, Carrica PM. Suggar++: An improved general overset
24
25
26 520 grid assembly capability. 19th AIAA Comput. Fluid Dyn. Conf., San Antonio, Texas,
27
28
29 521 USA: 2009.
30
31 522 [19] Cao H, Wan D. Application of OpenFOAM to simulate three-dimensional flows past a
32
33
34 523 single and two tandem circular cylinders. Proc. Int. Offshore Polar Eng. Conf., vol. 3,
35
36
37 524 2010, pp. 702–9.
38
39 525 [20] Zhou H, Cao H, Wan D. Numerical Predictions of Wave Impacts on the Supporting
40
41
42 526 Structures of Shanghai Donghai-Bridge Offshore Wind Turbines. Twenty-Third Int.
43
44
45 527 Offshore Polar Eng. Conf., Anchorage, Alaska, USA: International Society of Offshore
46
47
48 528 and Polar Engineers; 2013.
49
50 529 [21] Wang J, Zou L, Wan D. CFD simulations of free running ship under course keeping
51
52
53 530 control. Ocean Eng 2017;141:450–64.
54
55
56 531 [22] Liu M, Xiao L, Yang J, Tian X. Parametric study on the vortex-induced motions of
57
58

1 532 semi-submersibles: Effect of rounded ratios of the column and pontoon. *Phys Fluids*
2
3 533 2017;29:055101.
4
5
6 534 [23] Liang Y, Tao L. Interaction of vortex shedding processes on flow over a deep-draft
7
8
9 535 semi-submersible. *Ocean Eng* 2017;141:427–49.
10
11 536 [24] Antony A, Vinayan V, Holmes S, Spornjak D, Kim SJ, Halkyard J. VIM Study for Deep
12
13
14 537 Draft Column Stabilized Floaters. *Offshore Technol. Conf.*, Houston, Texas, USA: 2015.
15
16
17 538 [25] Waals OJ, Phadke AC, Bultema S. Flow induced motions of multi column floaters. *Proc.*
18
19
20 539 26th Int. Conf. Offshore Mech. Arct. Eng., vol. 1, San Diego, California, USA: 2007, p.
21
22
23 540 669–78.
24
25
26 541 [26] Rijken O, Leverette S. Experimental Study Into Vortex Induced Motion Response of Semi
27
28
29 542 Submersibles With Square Columns. *Proc. ASME 27th Int. Conf. Offshore Mech. Arct.*
30
31
32 543 *Eng.*, vol. 1, Estoril, Portugal: 2008, p. 263–76.
33
34 544 [27] Gonçalves RT, Nishimoto K, Rosetti GF, Fugarra ALC, Oliveira AC. Experimental study
35
36
37 545 on vortex-induced motions (VIM) of a large-volume semi-submersible platform. *Proc.*
38
39
40 546 ASME 2011 30th Int. Conf. Ocean Offshore Arct. Eng., vol. 7, Rotterdam, The
41
42
43 547 Netherlands: 2011, pp. 1–9.
44
45 548 [28] Zou J, Poll P, Roddier D, Tom N, Peiffer A. VIM testing of a paired column semi
46
47
48 549 submersible. *Proc. ASME 2013 32nd Int. Conf. Ocean Offshore Arct. Eng.*, vol. 7, Nantes,
49
50
51 550 France: 2013, p. V007T08A001.
52
53 551 [29] KHALAK A, WILLIAMSON CHK. MOTIONS, FORCES AND MODE TRANSITIONS
54
55
56 552 IN VORTEX-INDUCED VIBRATIONS AT LOW MASS-DAMPING. *J Fluids Struct*

1 553 1999;13:813–51.
2
3 554 [30] Gonçalves RT, Rosetti GF, Fajarra C, Luís A, Nishimoto K, Oliveira C. Vortex-Induced
4
5
6 555 Yaw Motion (VIY) of a Large-Volume Semi-Submersible Platform, Rhodes, Greece:
7
8
9 556 International Society of Offshore and Polar Engineers; 2012.
10
11 557 [31] Liu M, Xiao L, Liang Y, Tao L. Experimental and numerical studies of the pontoon effect
12
13
14 558 on vortex-induced motions of deep-draft semi-submersibles. J Fluids Struct 2017; 72:
15
16
17 559 59–79.
18
19
20 560